Bounding the Residual Tropospheric Error by Interval Analysis

Jingyao Su and Steffen Schön

Abstract

GNSS integrity monitoring requires proper bounding to characterize all ranging error sources. Unlike classical approaches based on probabilistic assumptions, our alternative integrity approach depends on deterministic interval bounds as inputs. The intrinsically linear uncertainty propagation with intervals is adequate to describe remaining systematic uncertainty, the so-called imprecision. In this contribution, we make a proposal on how to derive the required intervals in order to quantify and bound the residual error for empirical troposphere models, based on the refined sensitivity analysis via interval arithmetic. We evaluated experimentally the Saastamoinen model with (i) a priori ISO standard atmosphere, and (ii) on-site meteorological measurements from IGS and Deutscher Wetterdienst (DWD) stations as inputs. We obtain consistent and complete enclosure of residual ZPD errors w.r.t IGS ZPD products. Thanks to the DWD dense network, interval maps for meteorological parameters and residual ZPD errors are generated for Germany as by-products. These experimental results and products are finally validated, taking advantage of the high-quality tropospheric delays estimated by the Vienna Ray Tracer. Overall, the results indicate that our strategy based on interval analysis successfully bounds tropospheric model uncertainty. This will contribute to a realistic uncertainty assessment of GNSS-based single point positioning.

Keywords

Error bounding · Global navigation satellite systems · Integrity · Interval analysis · Residual tropospheric error

1 Introduction

Nowadays, GNSS is used for many safety-critical applications, such as aviation and autonomous driving, where the high-integrity performance of the navigation system must be ensured. To assess the integrity, i.e., the trust that we can put into a navigation solution, all contributing observation error sources are to be quantified and propagated to the position domain. A Protection Level (PL) is calculated as the bound on these propagated errors, including code noise and multipath, clock and orbit errors, residual ionospheric error, and residual tropospheric error (Rife et al. 2006). To avoid any underestimation of the PLs, these separate error sources need to be modeled and bounded properly.

As one of the primary error sources, the tropospheric error is in practice widely corrected by well-developed empirical troposphere models. For example, the Saastamoinen model is applied in a "blind" mode with a priori standard atmosphere, e.g., ISO2533 (ISO et al. 1995) or U.S. standard atmosphere, and the Global Pressure and Temperature model GPT2 (Lagler et al. 2013); the Radio Technical Commission for Aeronautics (RTCA) recommends the model of Askne

J. Su (✉) · S. Schön
Institut für Erdmessung, Leibniz Universität Hannover, Hannover, Germany
e-mail: suj@ife.uni-hannover.de; schoen@ife.uni-hannover.de

J. T. Freymueller, L. Sánchez (eds.), *Geodesy for a Sustainable Earth*,
International Association of Geodesy Symposia 154, https://doi.org/10.1007/1345_2022_184

and Nordius (1987) to estimate the wet delay for the minimum operational performance standard (MOPS) (RTCA-DO229 2006); these two models are also adopted in GPT2w (Böhm et al. 2015) and GPT3 (Landskron and Böhm 2018), fed with corresponding empirical meteorological models. The performance of these models must be evaluated, and the residual error must be modeled to ensure high-integrity navigation solutions.

Up until now, the residual tropospheric error is treated stochastically in almost all bounding methods, and subsequently a quadratic error propagation is applied. For example, MOPS indicates a maximum vertical error of 0.12 m in terms of standard deviation globally for its correction model (RTCA-DO229 2006); In aviation, the overbounding method is developed based on conservative approximations of cumulative density function (CDF) (DeCleene 2000; Rife et al. 2006); Rózsa (2018) and Rózsa et al. (2020) introduced the generalized extreme value theory to account for the tails of the distribution and developed residual tropospheric error models; Gallon et al. (2021) investigated time correlation modeling by bounding the autocorrelation function (ACF) and power spectral density (PSD). The resulting bounds on stochastic parameters for residual tropospheric errors are utilized in Kalman filters.

The methods mentioned above are applied almost exclusively in a stochastic manner. However, the exact error distribution is often unknown, and remaining systematic errors may persist so that alternative linear uncertainty propagation should be studied (Schön and Kutterer 2005). Unlike classical approaches based on probabilistic assumptions, the alternative integrity approach depends on deterministic interval bounds as inputs, which are usually defined as the maximum variation of the error in worst cases or with a confidence level under probabilistic assumptions (Dbouk and Schön 2019; Su and Schön 2022). Very few studies have yet focused on the determination of meaningful observation interval bounds in general and on interval bounding for residual tropospheric errors in particular. Schön and Kutterer (2006) introduced the method of sensitivity analysis to GNSS applications but still did not validate with real data.

This contribution, in response, will make a proposal on how to derive the required interval bounds based on interval analysis in order to quantify and bound the residual tropospheric error and validate it, as summarized in Fig. 1.

The remainder is organized as follows: Sect. 2 reviews the sensitivity analysis and refines it in view of interval arithmetic. Section 3 introduced the strategy how we estimate the uncertainty of model influence factors. In Sect. 4, we implement the proposed method with the Saastamoinen model with a priori standard atmosphere (ISO2533). We obtain the uncertainty of meteorological parameters taking advantage of IGS meteorological measurements as well as climate data from the Deutsche Wetterdienst (DWD). Interval maps for meteorological parameters and residual ZPD errors that assess their uncertainty are generated as by-products over Germany. Finally, we validate the resulting bounds through comparison of tropospheric delay residuals based on empirical cumulative functions in Sect. 5. Concluding remarks and an outlook are given in Sect. 6.

2 Methodology: Sensitivity Analysis

This section first summarizes the definitions and basic operations of intervals; next reviews the concept of sensitivity analysis that is applied in previous studies, and reformulate the method in view of interval arithmetic.

2.1 Basics of Interval Arithmetic

An interval is defined as $[x] = [\underline{x}, \overline{x}]$, with $\underline{x}$ being the lower bound and $\overline{x}$ upper bound.

For any bounded, and non-empty interval $[x]$, the midpoint $mid([x]) = x_m$ and radius $rad([x]) = x_r$ are defined as:

$$mid([x]) = x_m \triangleq \frac{\underline{x} + \overline{x}}{2}, \; rad([x]) = x_r \triangleq \frac{\overline{x} - \underline{x}}{2} \tag{1}$$

The real-valued arithmetic operations can be mostly extended to intervals, with the same basic operators: $+$, $-$, $\times$, $\div$, sin, tan, exp and so on:

$$[x] \diamond [y] = \{x \diamond y \in \mathbb{R} \mid x \in [x], y \in [y]\} \tag{2}$$

where $[x]$ and $[y]$ are intervals and $\diamond$ can be any of the algebraic operations listed above.

Similarly, an interval vector or interval matrix is higher dimensional, which are defined as the Cartesian product of n and $m \times n$ interval, separately.

If f represents a real-valued function of a single real variable x, the range of values determined by $f(x)$ as x varies within a given interval $[x]$ is the image of set $\{x|x \in [x]\}$ under mapping f:

$$f([x]) = \{f(x) \mid x \in [x]\} \tag{3}$$

Analogously, if f is a function of multiple real variable $\mathbf{x} = [x_1, ..., x_m]^T$, the output interval of f when its i-th variable x_i varies in an interval $[x_i]$ reads:

$$f([x_i] \mid \mathbf{x}^*) = \{f(\mathbf{x}) \mid x_i \in [x_i], \mathbf{x}_{(...,i-1,i+1,...)} = \mathbf{x}^*_{(...,i-1,i+1,...)}\}$$

in other words, the set image of $[x_i]$ under the mapping f; all other variables have their values from $\mathbf{x}^*$.

Interested readers will find more detailed introduction about interval computations in textbooks, e.g., Jaulin et al. (2001) and Moore et al. (2009).

2.2 Sensitivity Analysis in View of Intervals

Sensitivity analysis is a forward modeling approach to assess the uncertainty due to remaining systematic errors (ISO et al. 1995) and can be applied on GNSS observations (Schön and Kutterer 2006). The basic idea behind is as follows: the empirical models are built based on assumptions deviating from reality and approximations with uncertainty. Hence, the constants and parameters used in the models are often only imprecisely known and associated with a given range. Their uncertainties should contribute to a maximum range of variation (interval) for the model's output. This interval reflects the uncertainty due to remaining systematic errors.

To this end, the approach by Schön and Kutterer (2006) computes sensitivity coefficients through partial differentiation and subsequently computes an interval radius for the final uncertainty budget:

Consider a dedicated model f with m influence factors $\mathbf{x} = \{x_i, i = 1, ..., m\}$. For given values of $\mathbf{x} = \mathbf{x}^*$, and their uncertainty in terms of interval radii $\mathbf{x}_r$, the matrix of sensitivity coefficients $\mathbf{F}$ and final interval radius f_r read:

$$\mathbf{F} = \frac{\partial f(\mathbf{x}^*)}{\partial \mathbf{x}_r}, \quad f_r = |\mathbf{F}| \cdot \mathbf{x}_r \tag{4}$$

For this method, the partial differentiability of the dedicated model must be given, and uncertainties of influence factors are assumed to be small enough, which, however, are sometimes invalid.

To cope with this issue, we propose to implement the sensitivity analysis via interval arithmetic:

The model's uncertainty budget (interval value $[f]$) is expressed as the sum of all influence factors' contributions:

$$[f] \triangleq [\underline{f}, \overline{f}] = \sum_{i}^{m} [f_i] + f(\mathbf{x}^*) \tag{5}$$

with a lower bound ($\underline{f}$) and an upper bound ($\overline{f}$).

The sensitivity f_i of f w.r.t the change of one specific influence factor x_i in its interval $[x_i] \triangleq [\underline{\Delta x_i}, \overline{\Delta x_i}] + x_i^* = [\underline{x_i}, \overline{x_i}]$ is determined by:

$$[f_i] \triangleq f([x_i] \mid \mathbf{x}^*) - f(\mathbf{x}^*) \tag{6}$$

The uncertainty is evaluated via interval arithmetic instead of real-valued operations on interval radii, therefore, the resulting uncertainty intervals are not necessarily symmetric w.r.t $f(\mathbf{x}^*)$.

3 Estimate the Uncertainty of Model Influence Factors

It can be noticed from Sect. 2 that the key to the proposed interval-based sensitivity analysis is the reliable characterization of model's influence factors and the assessment of their uncertainties. This is because every single influence factor contributes an uncertainty interval to the overall budget, cf. Eqs. 5, 6.

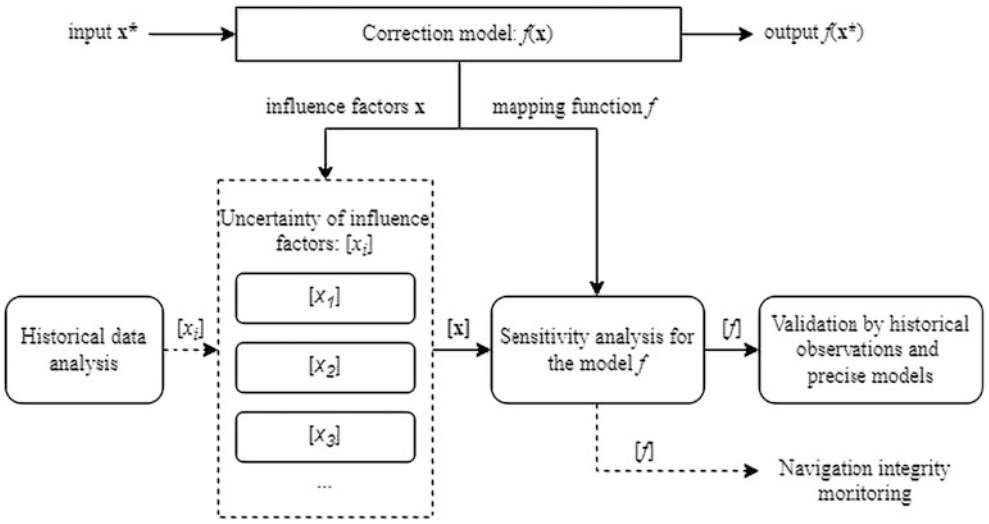

Fig. 1 Flowchart of the study: for a given correction model $f(\mathbf{x})$, we derive its sensitivity w.r.t all influence factors $[\mathbf{x}]$ mathematically and determine its uncertainty budget $[f]$ from all contributions. The outputs are interval bounds under dedicated condition for further integrity applications. They are validated in this study using historical data and precise models

According to JCGM (2008), the uncertainties of model influence factors are evaluated by scientific judgement based on all of the available information:

- uncertainty information indicated in the construction process of the model
- expert knowledge or experience of the behavior and properties of relevant factors
- manufacturer's specification
- information provided by model's accuracy evaluations
- uncertainties assigned to reference data taken from handbooks

This paper focuses on the Saastamoinen model (Saastamoinen 1972), which shows that the zenith tropospheric delay (ZPD) can be calculated from surface meteorological parameters as:

$$\Delta L = \beta_1 \frac{(1+\beta_2 \cos^2(\theta)+\beta_3 H)}{\cos(z)}[p + \beta_4 \frac{T}{e} + \beta_5 e - B\tan^2(z)] + \delta_r \tag{7}$$

where ΔL is the range correction, p is the pressure at the antenna site in hPa, e the partial water vapor pressure in hPa, T the absolute temperature in $Kelvin$, B and δ_r correction terms, $\beta_1, \beta_2, ..., \beta_5$ constants, and z the apparent zenith distance, determined from true zenith distance Z of the satellite by the formula $z = Z - \delta z$ with:

$$\delta_z = \frac{\alpha_1}{T}\tan(Z)(p + \frac{\alpha_2}{T}e) - \alpha_3 \tan(Z)(\tan^2(Z) + 1)\frac{p}{1000} \tag{8}$$

where $\alpha_1, \alpha_2, \alpha_3$ and α_4 are constant coefficients, and Z can be determined from the station height H in $meter$, station latitude ϕ in $degree$ and satellite elevation θ in $radius$. All the primary variables and constants above-mentioned constitute the vector of influence factors $\mathbf{x}$, cf. Eqs. 5, 6, for the Saastamoinen model: $\mathbf{x}_{SAAST} = [T, p, e, \alpha_1, \alpha_2, \alpha_3, \beta_1, \beta_2, \beta_3, \beta_4, \beta_5, H, \phi, \theta]^T$.

Any physical quantity should only be given with a meaningful number of digits. Half of the last digit of the quantity is often referred to as rounding error. We follow this concept at the first step, assigning an uncertainty due to rounding error to all influence factors of the Saastamoinen model $\mathbf{x}_{SAAST}$. This corresponds to the radii of symmetric intervals, cf. Sect. 2.2. For example, Dbouk and Schön (2019) suggests $Rad([p]) = 0.5 \cdot 10^{-4}$, when the input value for surface pressure is provided 4-digit.

However, this evaluation of uncertainty may not be realistic, sometimes too optimistic. The actual range of variation for some factors may have a different order of magnitude. In the case of the Saastamoinen model, researchers have studied the uncertainty of a constant coefficient $\beta_1 = 2.277 \cdot 10^{-3}$: an error bar of $0.5 \cdot 10^{-6}$ is given by Davis et al. (1985); Zhang et al. (2016) suggests a value of $2.2794 \cdot 10^{-3}$. We adopt a larger value for its interval radius, i.e., the difference of the suggested value to original one plus rounding error, $Rad([\beta_1]) = (2.4 + 0.5) \cdot 10^{-6}$, indicating the maximum range of variation of β_1.

Additional care must be paid to the meteorological parameters, because they are inputs of the model and they vary temporally and spatially, having significant influence on the model's output. According to Feng et al. (2020), the pressure measurements at ground level are less representative of the "true" mean surface pressure than those at a higher level, probably due to turbulence. This will introduce uncertainty to the Saastamoinen model. Therefore, we propose performing long-term statistics against on-site meteorological measurements to estimate their interval bounds. In this contribution, the ISO2533 standard atmosphere is used as the a priori parameters to feed the Saasatamoinen model. We define a sliding window of two consecutive months on the time series and from each window, we take all the difference values of the standard atmosphere w.r.t the on-site measurements. The window slides in daily steps. Next, the upper and lower bounds of an interval are derived as a pair of quantiles of data within the sliding window. The quantile pairs should be determined based on the requirement of applications, e.g., [5%, 95%], [0.15%, 99.85%] and minimum/maximum values etc. In this way, daily interval bounds are obtained, i.e., $[p]$, $[T]$, and $[e]$.

Figure 2 shows the example results for the IGS stations Potsdam (POTS, a-1, b-1 and c-1) and Oberpfaffenhofen (OBE4, a-2, b-2 and c-2) during the year 2020: residuals of the ISO standard atmosphere (w.r.t on-site measurements, dots in grey) and interval bounds (colored curves) for those parameters, i.e., temperature (T), surface pressure (p) and water vapor pressure (e). The bounds of min/max values are wider, enclosing all the residuals, while the bounds of quantile pairs are relatively narrower, and violated by occasional extreme values.

4 Assessment of Residual Tropospheric Error

After having obtained uncertainty intervals of all influence factors $\mathbf{x}_{SAAST}$, the sensitivity analysis is implemented for the Saastamoinen model via interval arithmetic based on Eq. 6, resulting in $S_f(x_{SAAST,i})$, the sensitivity of the model f_{SAAST} w.r.t to each of the 14 elements of $\mathbf{x}_{SAAST}$. Subsequently, $[f_{SAAST}]$, the interval bounds for residual tropospher-ic errors are computed based on Eq. 5.

To demonstrate results, we compute ZPD residuals, defined as the difference of computed ZPD from the Saastamoinen model w.r.t reference estimates. By definition, the

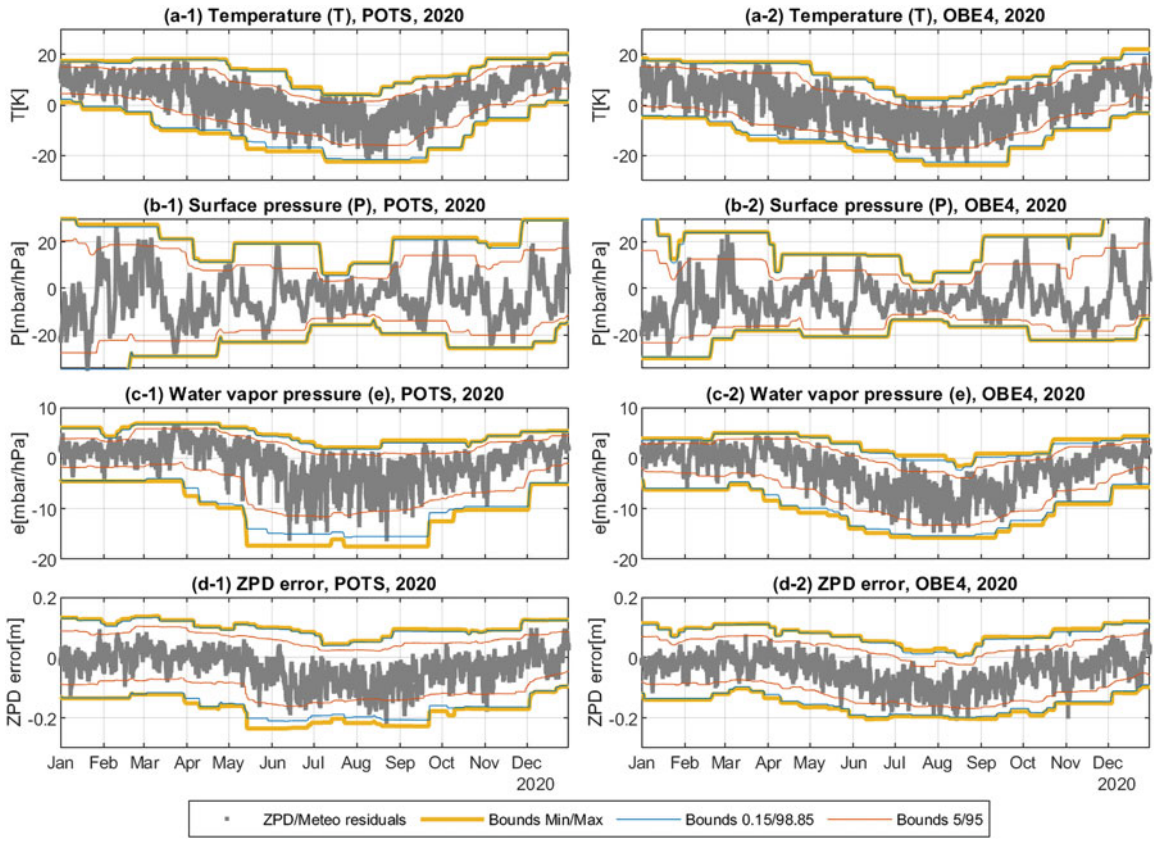

Fig. 2 Example results of IGS station POTS (left) and OBE4 (right) in 2020: residuals (ISO-to-RNX) and bounds for meteorological parameters (temperature, pressure, partial water vapour) from long-term statistics. ZPD bounds are computed with these results, and compared to residuals (Saastamoinen with ISO-to-IGS ZPD)

actual "residual ZPD error" is referenced to the truth. For IGS stations POTS and OBE4, we take the IGS ZPD products as reference. In Fig. 2 (d-1, d-2), the residuals are shown as grey dots, compared with the assessed interval bounds (colored curves, obtained with corresponding meteorological interval bounds). We expect complete enclosure of grey dots by colored curves. Obviously, this is the case for the widest interval bounds at POTS station, obtained with min/max meteorological interval bounds. As a comparison, other bounds, computed from quantile pairs, are narrower but may be exceeded by the residuals. For the OBE4 station, an exception can be observed on Nov. 4, 2020, during a short period of which the residuals are not enclosed by any bounds. The cause might be any perturbation occurring in the atmosphere, which cannot be captured by the surface measurements. The uncertainty for meteorological parameters is subsequently underestimated at these epochs, resulting in failures in ZPD bounding. This issue should be resolved in future works by refining the estimation for the uncertainty of relevant influence factors.

In addition, Deutscher Wetterdienst (DWD) operates a dense network of climate sensors over Germany, faciliting the analysis for multiple stations and the estimation for the geographical distribution of error bounds over the country. We applied a linear interpolation to the scattered dataset and obtained a $0.25° \times 0.25°$ gridded network. Example results for three meteorological parameters on the day 239 of 2020 are shown in Fig. 3. Using these interval bounds as input to the proposed sensitivity analysis, the interval maps for residual ZPD errors are obtained, cf. Fig. 4. Cross-sections of the interval maps in Fig. 4 along 9.7°E and 11.3°E meridians, which cross Hannover and Potsdam, are presented in Fig. 5. From these figures, we are interested in seeking potential dependency of the uncertainty intervals for residual ZPD error on meteorological parameters in terms of their geographical distributions. There are some interesting remarks:

– The "wet" troposphere dominates the overall interval bound, (i) similar pattern of two-dimensional geographical distribution can be found between water vapor pressure (cf. Fig. 3) and residual ZPD error (cf. Fig. 4), (ii) similar tendency of their one-dimensional latitudinal variation can also be observed in Fig. 5.
– Empirical tropospheric correction models may not capture the impact of regional, small-scaled weather events, during which the interval bounds should be expanded

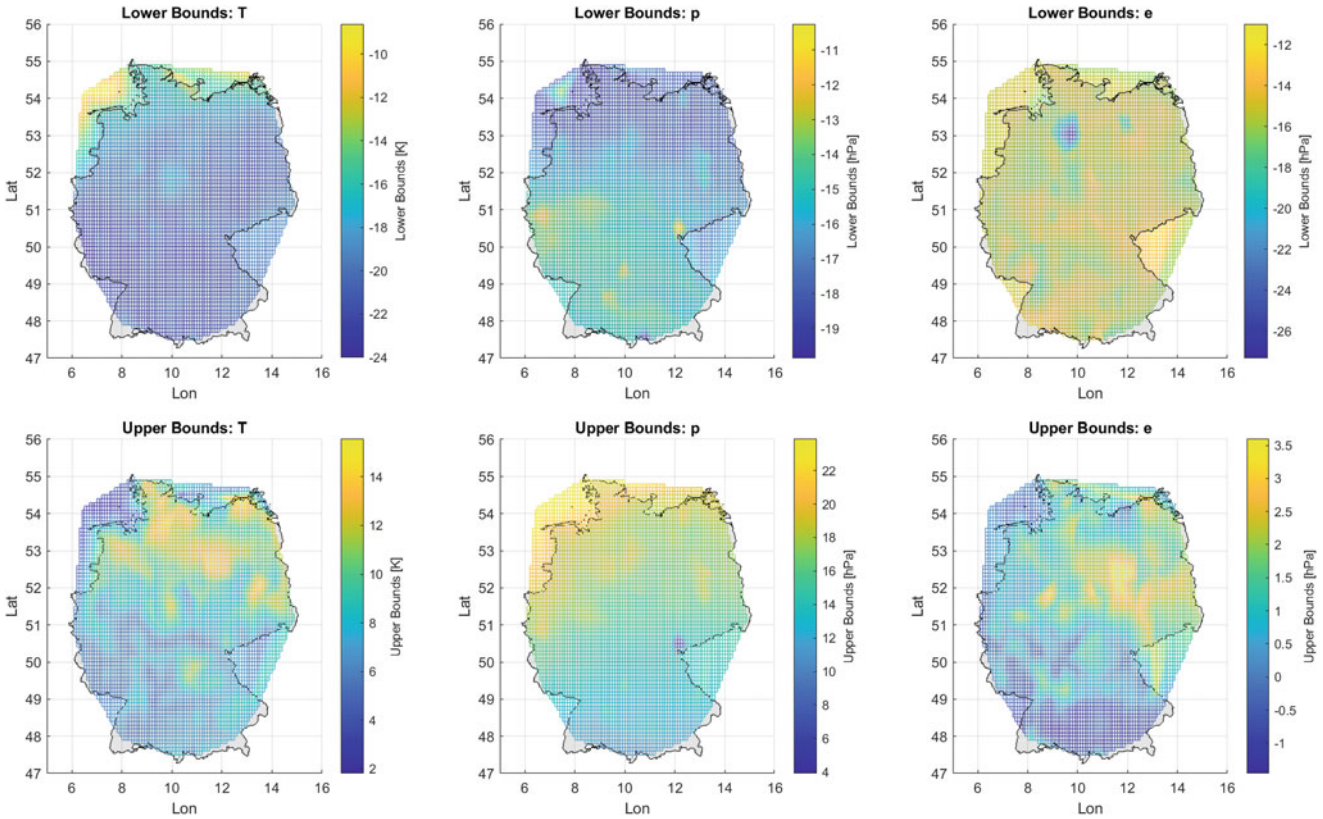

Fig. 3 Geographical distribution of lower interval bounds (upper column) and upper interval (lower column) bounds (right) for meteorological parameters over Germany on DOY 239 in 2020. The interval bounds are obtained based on statistics for on-site measurements from 215 out of 345 DWD stations

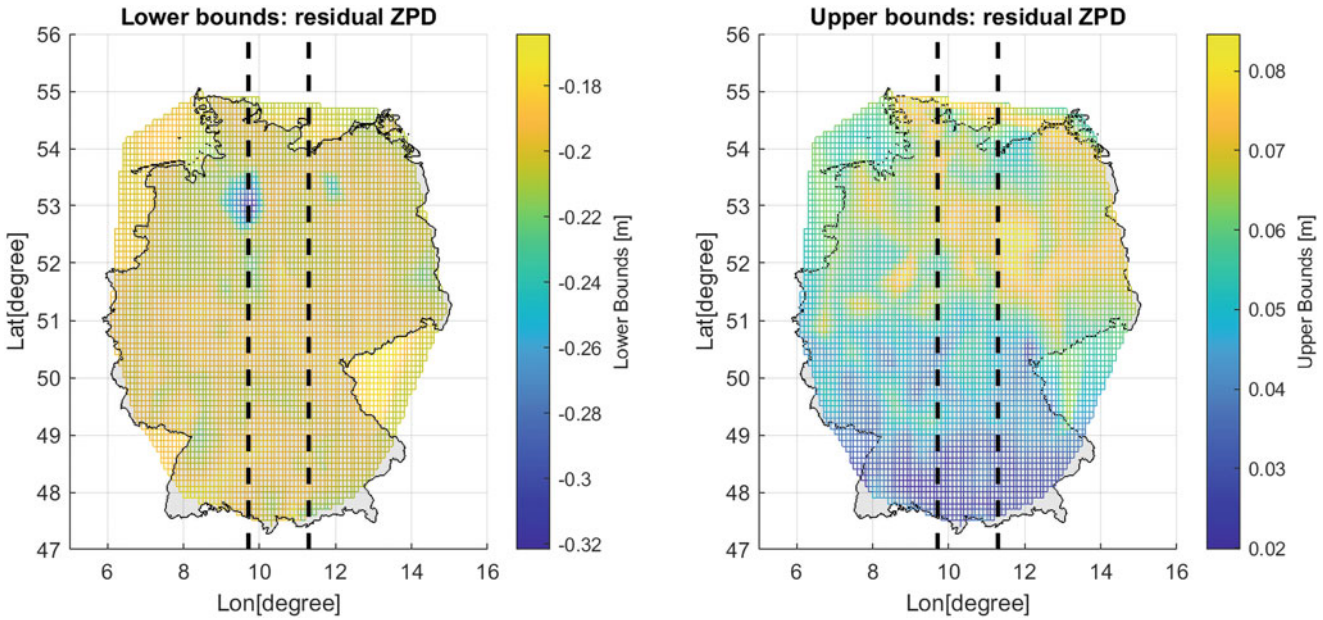

Fig. 4 Geographical distribution of lower interval bounds (left) and upper interval bounds (right) for bounding the residual ZPD error over Germany on DOY 239 in 2020. The computation is based on the proposed sensitivity analysis of the Saastamoinen model using interval bounds from Fig. 3

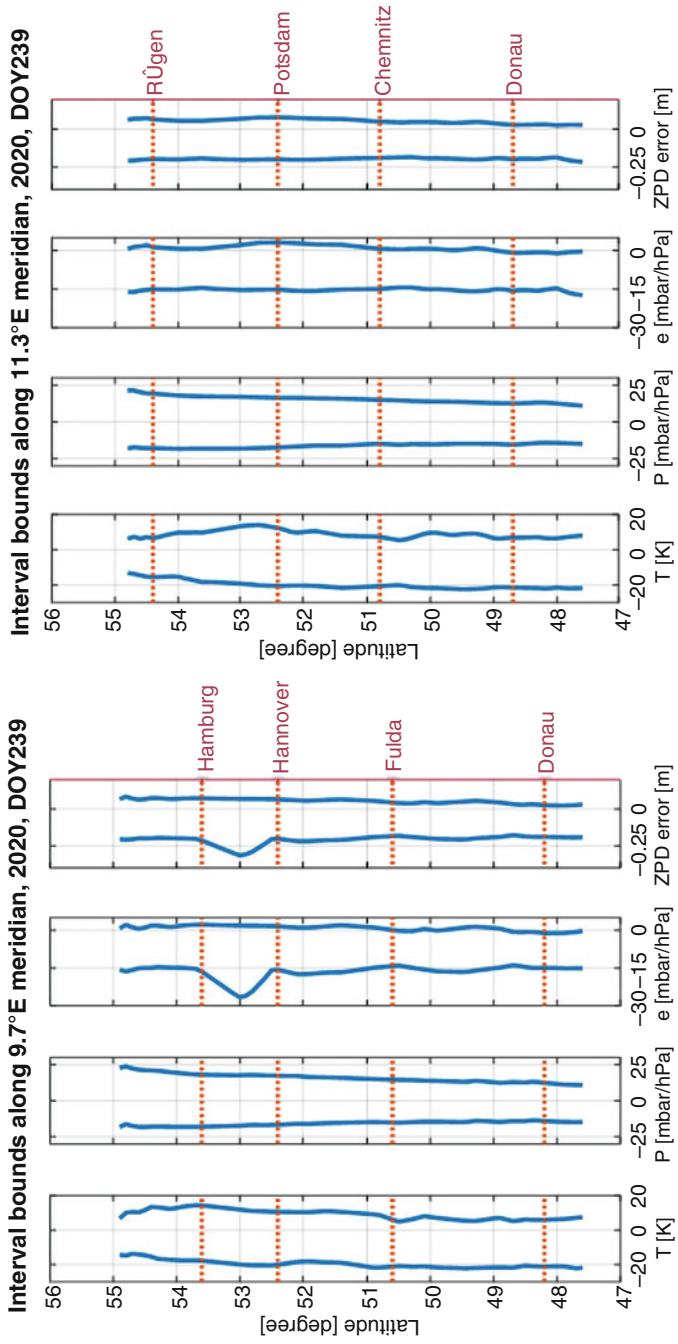

Fig. 5 Example results: interval bounds for meteorological parameters (from ISO-to-DWD) and ZPD (Saastamoinen with ISO) along the 9.7°E and 11.3°E meridians (denoted in Fig. 4 as black dashed lines) on DOY 239 in 2020. Climate data source: Deutscher Wetterdienst (DWD)

correspondingly. This is visible in Fig. 5: the region between Hamburg and Hannover indicates significant wider intervals for water vapor pressure and residual ZPD error. Counterparts exist in the interval maps in Fig. 4.

– The interval maps for residual ZPD errors show good agreements with the station-wise experimental results. We take POTS station on day 239 of 2020 as an example, which is visible in both of Fig. 2 (d-1, Oct. 26th on x-axis) and Fig. 5 (right, the fourth sub-figure, 52.379°N on y-axis): they are assessed based on different uncertainty evaluation for meteorological parameters (Fig. 2 using on-site measurements directly, and Fig. 5 using interpolated values from sensor network), nevertheless, resulting in very close interval values. In fact, we also tested with the other station OBE4 and with more days, showing the difference of ZPD bounds of mm to 10 mm level.

5 Validation

In this section, we aim to evaluate how well the bounds enclose potential deviations of the model outputs (e.g., Saastamoinen model with ISO) from reality. Since ground truth for tropospheric delays is difficult to achieve, we take (i) the IGS ZPD products and (ii) estimates from Vienna Ray-Tracer (RT) as reference. The ray-tracing technique directly reconstructs the true signal path and subsequently computes the atmospheric delay along the path based on numerical weather models, hence provides high-quality ZPD and SPD (slant directions) estimation (Hofmeister and Böhm 2017). However, this approach is computational expensive and has a relatively low temporal resolution (6 h), which prevents its usage in real-time applications. We additionally analyze the Saastamoinen model with inputs of on-site meteorological measurements (RNX) for comparison. Intervals for influence factors and subsequently for residual ZPD errors are determined with same methods, and again referred to IGS ZPD products as well as ray-traced delays.

We define bound-minus-residual (BMR) values, i.e., $\underline{\Delta}, \overline{\Delta}$, as the over-bounding indicator:

$$\underline{\Delta} = \underline{f} - (T_M - T_R), \quad \overline{\Delta} = \overline{f} - (T_M - T_R) \tag{9}$$

where $\underline{f}$ and $\overline{f}$ are lower and upper bounds of the intervals, T_M and T_R denote the modeled troposphere correction and reference delay, respectively. The BMR naturally indicates over-bounding performance for dedicated interval bounds, i.e., $\overline{\Delta}$ is supposed to have positive sign and $\underline{\Delta}$ negative, while both are expected close to zero ideally. Computing a large amount of data, it would be beneficial to observe the statistical parameters, e.g., the empirical cumulative density function (ECDF). Two key aspects regarding ECDF curves are of interest:

1. Success of bounding: whether the bounds sufficiently enclose all residuals, i.e., positive $\overline{\Delta}$ and negative $\underline{\Delta}$
2. Conservativity of over-bounding: the width of margin between the bounds and residuals in case of successful bounding, i.e., the deviation of curves from the y-axis

The ECDF curves for all scenarios for POTS are presented in Fig. 6. We show the values of the 90% percentile and min/max intervals of all ECDF in Table 1. The 90% bound is also indicated as a horizontal dashed red line in Fig. 6. It is worth noting that:

– An input of whether standard atmosphere or on-site meteorological measurements to the Saastamoinen model makes few difference to the uncertainty budget of residual tropospheric errors, no matter in zenith direction, or in slant directions. This is because the inputs to the Saastamoinen model are representative values. Neither of them is advantageous in uncertainty due to the construction process of the model.

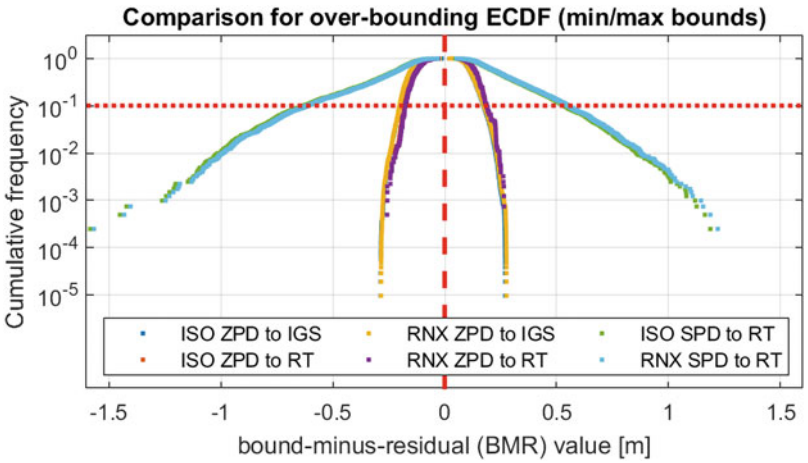

Fig. 6 ECDF of BMR values ($[\underline{\Delta}, \overline{\Delta}]$) for POTS station. The input meteorological data is from either standard atmosphere (ISO) or on-site measurements (RNX); the tropospheric delay residuals are from either zenith delays (ZPD) or slant delays (SPD); the reference data is from either IGS ZPD products (IGS) or Ray-Tracing Technique (RT). 90% of the values are located above the red dashed line

Table 1 90% and min/max interval of ECDF for BMR values ($[\underline{\Delta}, \overline{\Delta}]$) for six scenarios as defined in Fig. 6: 90%, or all of BMR are inside such an interval

Scenario	90% interval [m]	min/max interval [m]
ISO-ZPD-IGS	[−0.201, 0.174]	[−0.286, 0.271]
ISO-ZPD-RT	[−0.179, 0.182]	[−0.260, 0.260]
RNX-ZPD-IGS	[−0.201, 0.176]	[−0.284, 0.276]
RNX-ZPD-RT	[−0.175, 0.187]	[−0.257, 0.266]
ISO-SPD-RT	[−0.626, 0.537]	[−1.582, 1.322]
RNX-SPD-RT	[−0.613, 0.551]	[−1.566, 1.353]

- Being referred to whether the IGS ZPD products or ray-traced delays, the BMR shows a slight difference in ECDF curves. Both reference data are of high-quality, thus can be cross-checked.
- The ECDF curves are not necessarily symmetric to the y-axis, because (i) the accuracy of reference is never perfect, and (ii) some influence factors being aligned with symmetric uncertainty intervals may not be adequately assessed. For example, the absolute values $|\underline{\Delta}|$ are usually greater than $|\overline{\Delta}|$ in zenith direction for IGS-referenced scenarios (dark blue and yellow). Meanwhile, this is not necessary the case of RT-referenced curves (green, orange, purple and light blue), which are shifted around 2 cm to the right side w.r.t IGS-referenced ones.
- Mapping function: we didn't make an evaluation on the impact of mapping functions in the proposed method but directly inflate the intervals with corresponding mapping factors for slant directions. Therefore, the ECDF curves for SPD (green an light blue) are significantly wider than those for ZPD. Nevertheless, the impact of uncertainty due to mapping functions may be observed from, i.e., the change of asymmetry of ECDF curves from zenith to slant directions: in Table 1, we notice $|\underline{\Delta}| \leq |\overline{\Delta}|$ for "ISO-ZPD-RT" and "RNX-ZPD-RT" for 90% and min/max intervals, while "ISO-SPD-RT" and "RNX-SPD-RT" are in the opposite situation, i.e., $|\underline{\Delta}| > |\overline{\Delta}|$. This finding suggests the presence of systematic error due to mapping functions, which has to be captured by an additional interval.

6 Conclusions and Outlook

Taking the example of the Saastamoinen model, our implementation indicates the feasibility of the proposed method in qualifying and bounding residual tropospheric errors, based on sensitivity analysis via interval arithmetic. To evaluate the bounding performance, we computed bound-minus-residual (BMR) values as over-bounding indicators. Either standard atmosphere or on-site meteorological measurements are input to the Saastamoinen model. Tropospheric delay estimates provided by the IGS and Vienna Ray-Tracer are taken as reference value. All ZPD and SPD residuals were successfully bounded for test data at POTS station. 90% of the over-bounding BMR values for ZPD are no greater than around 0.2 m.

Uncertainties of the model influence factors must be carefully assessed. The estimation for meteorological parameters is done through long-term statistics against on-site measurements. The usage of on-site measurements facilitates the modeling and bounding of seasonal and geographical dependency. Taking advantage of a dense network of climate sensors such as Deutscher Wetterdienst (DWD), we showed the generation of interval maps to assess the uncertainty for meteorological parameters and residual ZPD errors.

Further work will focus on the potential impact of the mapping functions, as well as the implementation of other empirical tropospheric correction models.

Acknowledgements This work was supported by the German Research Foundation (DFG) as part of the Research Training Group i.c.sens [RTG 2159].

The authors gratefully acknowledge Deutscher Wetterdienst (DWD) for providing climate data, Helmholtz-Centre Potsdam GFZ German Research Centre for Geosciences for providing measurement data at POTS and OBE4 stations, International GNSS Service (IGS) for providing GNSS data and products, TU Wien for providing access to the online Ray-Tracer.

References

Askne J, Nordius H (1987) Estimation of tropospheric delay for microwaves from surface weather data. Radio Science 22(03):379–386. https://doi.org/10.1029/RS022i003p00379

Böhm J, Möller G, Schindelegger M, Pain G, Weber R (2015) Development of an improved empirical model for slant delays in the troposphere (GPT2w). GPS Solutions 19(3):433–441. https://doi.org/10.1007/s10291-014-0403-7

Davis JL, Herring TA, Shapiro II, Rogers AEE, Elgered G (1985) Geodesy by radio interferometry: Effects of atmospheric modeling errors on estimates of baseline length. Radio Science 20(6):1593–1607. https://doi.org/10.1029/RS020i006p01593

Dbouk H, Schön S (2019) Reliability and integrity measures of GPS positioning via geometrical constraints. In: Proceedings of the 2019 international technical meeting of the institute of navigation, pp 730–743. https://doi.org/10.33012/2019.16722

DeCleene B (2000) Defining pseudorange integrity-overbounding. In: Proceedings of the 13th international technical meeting of the satellite division of the institute of navigation (ION GPS 2000), pp 1916–1924

Feng P, Li F, Yan J, Zhang F, Barriot JP (2020) Assessment of the accuracy of the Saastamoinen model and VMF1/VMF3 mapping functions with respect to ray-tracing from radiosonde data in the framework of GNSS meteorology. Remote Sensing 12(20):3337. https://doi.org/10.3390/rs12203337

Gallon E, Joerger M, Pervan B (2021) Robust modeling of GNSS tropospheric delay dynamics. IEEE Trans Aerospace Electron Syst 57(5):2992–3003. https://doi.org/10.1109/TAES.2021.3068441

Hofmeister A, Böhm J (2017) Application of ray-traced tropospheric slant delays to geodetic VLBI analysis. J Geodesy 91(8):945–964. https://doi.org/10.1007/s00190-017-1000-7

ISO, IEC, OIML, BIPM (1995) Guide to the expression of uncertainty in measurement. Geneva, Switzerland 122:16–17

Jaulin L, Kieffer M, Didrit O, Walter E (2001) Applied interval analysis: With examples in parameter and state estimation, robust control and robotics. Springer, London

JCGM (2008) Evaluation of measurement data - guide to the expression of uncertainty in measurement: JCGM 100:2008 (GUM 1995 with minor corrections)

Lagler K, Schindelegger M, Böhm J, Krásná H, Nilsson T (2013) GPT2: Empirical slant delay model for radio space geodetic techniques. Geophys Res Lett 40(6):1069–1073. https://doi.org/10.1002/grl.50288

Landskron D, Böhm J (2018) VMF3/GPT3: refined discrete and empirical troposphere mapping functions. J Geodesy 92(4):349–360. https://doi.org/10.1007/s00190-017-1066-2

Moore RE, Kearfott RB, Cloud MJ (2009) Introduction to interval analysis. SIAM

Rife J, Pullen S, Enge P, Pervan B (2006) Paired overbounding for nonideal laas and waas error distributions. IEEE Trans n Aerospace Electronic Syst 42(4):1386–1395. https://doi.org/10.1109/taes.2006.314579

Rózsa S (2018) A new approach for assessing tropospheric delay model performance for safety-of-life GNSS applications. In: Heck A, Seitz K, Grombein T, Mayer M, Stövhase JM, Sumaya H, Wampach M, Westerhaus M, Dalheimer L, Senger P (eds) (Schw)Ehre, wem (Schw)Ehre gebührt : Festschrift zur Verabschiedung von Prof. Dr.-Ing. Dr. h.c. Bernhard Heck, KIT Scientific Publishing. https://doi.org/10.5445/IR/1000080241

Rózsa S, Ambrus B, Juni I, Ober PB, Mile M (2020) An advanced residual error model for tropospheric delay estimation. GPS Solutions 24(4):1–15. https://doi.org/10.1007/s10291-020-01017-7

RTCA-DO229 (2006) Minimum operational performance standards for global positioning system/wide area augmentation system airborne equipment. RTCA

Saastamoinen J (1972) Contributions to the theory of atmospheric refraction. Bulletin Géodésique (1946–1975) 105(1):279–298. https://doi.org/10.1007/bf02521844

Schön S, Kutterer H (2005) Realistic uncertainty measures for GPS observations. In: Sansò F (ed) A window on the future of geodesy, international association of geodesy symposia, vol 128. Springer, Berlin/Heidelberg, pp 54–59. https://doi.org/10.1007/3-540-27432-4_10

Schön S, Kutterer H (2006) Uncertainty in GPS networks due to remaining systematic errors: The interval approach. J Geodesy 80(3):150–162. https://doi.org/10.1007/s00190-006-0042-z

Su J, Schön S (2022) Deterministic approaches for bounding GNSS uncertainty: A comparative analysis. In: 2022 10th workshop on satellite navigation technology (NAVITEC), pp 1–8. https://doi.org/10.1109/NAVITEC53682.2022.9847545

Zhang D, Guo J, Chen M, Shi J, Zhou L (2016) Quantitative assessment of meteorological and tropospheric zenith hydrostatic delay models. Adv Space Res 58(6):1033–1043. https://doi.org/10.1016/j.asr.2016.05.055